Molybdenum dynamics in sediments of a seasonally-hypoxic coastal marine basin

Fatimah Sulu-Gambari[1*], Anne Roepert[1], Tom Jilbert[1,2], Mathilde Hagens[1], Filip J. R. Meysman[3] and Caroline P. Slomp[1]

[1]Department of Earth Sciences (Geochemistry), Faculty of Geosciences, Utrecht University, P.O. Box 80.021, 3508 TA Utrecht, the Netherlands

[2]Department of Environmental Sciences, Faculty of Biological and Environmental Sciences, University of Helsinki, Finland

[3] NIOZ Royal Netherlands Institute for Sea Research, Department of Estuarine and Delta Systems, P.O. Box 140, 4400 AC Yerseke, the Netherlands, and Utrecht University.

*Corresponding author: tel: + 31 30 253 5037; e-mail: fatimah.sulu-gambari@uu.nl

Keywords: molybdenum, manganese oxides, sulphide, sediment, cable bacteria

Abstract

Molybdenum (Mo) enrichments in marine sediments are a common indicator of the presence of sulphide near the sediment-water interface and can thereby record historic bottom-water oxygen depletion. Here, we assess the impact of temporal changes in manganese (Mn) cycling and bottom-water oxygen on sedimentary Mo dynamics in a seasonally-hypoxic coastal marine basin (Lake Grevelingen, the Netherlands). High resolution line scans obtained with LA-ICP-MS and discrete sample analyses reveal distinct oscillations in Mo with depth in the sediment. These oscillations and high sediment Mo concentrations (up to ~130 ppm) are attributed to deposition of Mo-bearing Mn-oxide-rich particles from the overlying water, the release of molybdate (MoO_4^{2-}) to the pore water upon reduction of these Mn-oxides, and subsequent sequestration of Mo. The latter process only occurs in summer when sulphide concentrations near the sediment-water interface are elevated. We hypothesise that cable bacteria enhance the seasonality in sediment Mo records by contributing to remobilisation of Mo as MoO_4^{2-} during oxic periods and by enhancing the pool of Mn-oxides in the system by dissolving Mn-carbonates. A sediment record that spans the past ~45 years indicates that sediment Mo concentrations have increased over the past decades, despite less frequent occurrences of anoxia in the bottom waters based on oxygen measurements from water column monitoring. We suggest that the elevated Mo in recent sediments reflects both enhanced rates of sulphate reduction and sulphide production in the surface sediment as a result of increased input of organic matter into the basin from the adjacent North Sea since 1999, and an associated enhanced “Mn refluxing” in the marine lake in summer.

1. Introduction

Molybdenum (Mo) is the most abundant trace metal in the modern ocean (105 nM (Collier, 1985)) but is only a minor constituent of the Earth's crust (1-2 ppm; (Turekian and Wedepohl, 1961)). This discrepancy reflects the fact that molybdate (MoO_4^{2-}) behaves conservatively in oxic seawater, leading to an accumulation of Mo in the oceans and a residence time of ~4.4×10^5 years (Miller et al., 2011). However, Mo can be removed from seawater to marine sediments in the presence of hydrogen sulphide (H_2S), making sedimentary Mo an important proxy for past redox conditions. Under sulphidic conditions, multiple thiomolybdate intermediates ($MoO_xS_{4-x}^{2-}$) (Erickson and Helz, 2000; Helz et al., 1996) and complexes of Mo with organic ligands (Wagner et al., 2017) can form. However, when H_2S concentrations in seawater or pore water exceed ~11 µM, complete conversion to tetrathiomolybdate (MoS_4^{2-}) is thought to occur (Erickson and Helz, 2000; Helz et al., 1996; Wagner et al., 2017). Molybdenum can subsequently be sequestered through multiple co-occurring pathways involving organic matter, Fe phases and/or authigenic sulphides (Algeo and Tribovillard, 2009; Chappaz et al., 2014; Dahl et al., 2017; Freund et al., 2016; Tribovillard et al., 2006; Wagner et al., 2017). As long as the supply of Mo to the seawater in a given environment is not restricted (Algeo and Lyons, 2006), the redox-sensitive behaviour of Mo allows discrimination between two distinct bottom-water oxygen regimes. More specifically, depositional settings with oxic bottom waters in which sulphide is limited to pore waters throughout the year (sediment Mo < 25 ppm) can be separated from those characterised by permanent anoxic and sulphidic conditions (i.e. euxinia) in bottom waters (sediment Mo > 100 ppm (Scott and Lyons, 2012)).

Bottom-water hypoxia (O_2 < 62.5 µM (Levin et al., 2009; Rabalais et al., 2010)) has become increasingly prevalent in coastal environments worldwide over the past decades. This has led to so-called "dead zones", where the sediment and bottom-water are devoid of larger fauna (Diaz and Rosenberg, 2008; Rabalais et al., 2014). The increase in these dead zones is

often directly linked to increased nutrient input from land, which fuels algal blooms, thus enhancing the oxygen demand in deeper waters when algal material sinks to the seafloor (Carstensen et al., 2014; Diaz and Rosenberg, 2008). Sediment Mo records can provide valuable information on the timing of the onset of human-induced hypoxia, anoxia or euxinia and its further development (Gooday et al., 2009; Helz and Adelson, 2013). In the deep basins of the Baltic Sea, for example, a strong enrichment of Mo is observed in the upper ~20 cm of the sediment (up to ~220 ppm), in accordance with the establishment of euxinic conditions in the bottom waters of these basins since ~1980 (Jilbert and Slomp, 2013b; Mort et al., 2010; Scholz et al., 2013). Similarly, the expansion of hypoxic bottom waters in Chesapeake Bay since 1960 has been linked to an increased burial of Mo in the sediment (Adelson et al., 2001b; Helz and Adelson, 2013; Olson et al., 2017).

In non-euxinic settings, there are two main sources of Mo to sediments. First, MoO_4^{2-} may diffuse into sediments from the overlying water where it may be sequestered in H_2S-bearing pore waters (e.g. (Emerson and Huested, 1991; Tribovillard et al., 2006; Zheng et al., 2000)). Second, manganese-oxide particles may act as a major carrier of Mo to the sediment (Adelson et al., 2001b; Algeo and Lyons, 2006; Scheiderich et al., 2010). The input of Mo associated with Mn oxides can lead to two vertically-separated sediment enrichments in Mo: (1) an enrichment associated with Mn oxides at or near the sediment-water interface that is only a transient sink for Mo, and (2) an enrichment of Mo associated with sulphur and/or organic matter at depth that acts as a permanent sink (Morford et al., 2007; Scott and Lyons, 2012). Such dual Mo enrichments can be a permanent feature in sediments with oxic bottom waters (Malcolm, 1985). The release of Mo from Mn-oxides near the sediment-water interface may support a flux of Mo from the sediment to the overlying water. Such an efflux of Mo will prevent diffusion of Mo into the sediment (e.g. (Scott and Lyons, 2012)). In seasonally-hypoxic settings, the remobilisation of dissolved Mn from sediments, formation of Mn oxides in the

water column and re-deposition of Mo-bearing Mn-oxides on the sediment in summer may lead to such a high input of Mo that the diffusive loss of MoO_4^{2-} becomes unimportant relative to its input and conversion to tetrathiomolybdate (e.g. (Adelson et al., 2001a)). This so-called "Mn-refluxing" is thought to contribute to the high Mo burial fluxes in environments with weakly sulphidic bottom waters (Algeo and Lyons, 2006). To our knowledge, there are no detailed seasonal studies of the dynamics of Mo and Mn in both pore waters and sediments of hypoxic systems to confirm the suggested seasonality in coupled Mn-Mo cycling.

Recently, it was discovered that sulphide-oxidising cable bacteria (Nielsen et al., 2010; Pfeffer et al., 2012) may dissolve Fe-sulphides and Mn-carbonates in surface sediments of seasonally-hypoxic systems. Consequently, these bacteria actively contribute to the formation of an oxidised, Fe- and Mn-oxide rich surface layer in winter and spring (Seitaj et al., 2015; Sulu-Gambari et al., 2016b; Sulu-Gambari et al., 2016a). In contrast, sulphur oxidising Beggiatoaceae, present in autumn, had a more limited effect on the formation of Fe- and Mn-oxides in the surface sediment (Seitaj et al., 2015; Sulu-Gambari et al., 2016b; Sulu-Gambari et al., 2016a). Due to the coupling of Mn, Fe, S and Mo cycles in hypoxic systems, we hypothesise that the activity of cable bacteria may also be of relevance to the sedimentary dynamics of Mo. More specifically, we hypothesise that cable bacteria activity may amplify seasonal oscillations in sediment Mo linked to bottom-water hypoxia. This hypothesis is based on their role in the efficient re-dissolution of sulphide-associated Mo in winter and spring, and in enhancing the pool of Mn-oxides by dissolving Mn-carbonates (Rao et al., 2016; Sulu-Gambari et al., 2016b).

Here, we investigate the evolution of sediment and pore-water Mo profiles over one year in a seasonally hypoxic marine basin (Lake Grevelingen, the Netherlands). We focus on identifying the relationship between seasonal and spatial differences in bottom-water oxygen and the dynamics of Mo and Mn in the sediment. We assess whether sulphide-oxidising cable

bacteria and Beggiatoaceae, which are both known to be present in our study basin for at least part of the year (Seitaj et al., 2015; Sulu-Gambari et al., 2016b; Sulu-Gambari et al., 2016a) can impact the sequestration of Mo in the sediment. Our results reveal strong annual oscillations in sedimentary Mo content driven by seasonal hypoxia and amplified by Mn refluxing and the activity of sulphide-oxidising bacteria. Furthermore, using an extended sediment record for the past 45 years we show how the long-term evolution of sedimentary Mo content reflects changes in pore water sulphide concentrations and Mn refluxing.

2. Methods

2.1. Study sites and sample collection

Lake Grevelingen (Figure 1) is a former estuary of the rivers Rhine and Meuse. The lake was formed by the construction of a landward dam (1965) and seaward dam (1971) in response to flooding caused by a storm surge (1953). The shallow lake covers an area of 115 km^2 and has an average depth of 5.1 m but is intersected by several channels, of which the deepest (main channel) has a maximum water depth of 48 m (Figure 1) (Hagens et al., 2015; Sulu-Gambari et al., 2016b). The salinity of the lake falls within a stable range of 29 to 32 that is maintained via an exchange with the saline water from the North Sea through an underwater sluice in the Brouwersdam (Paulij et al., 1990). In spring and summer a temperature-dependent stratification develops in the main channel (Hagens et al., 2015). Bottom-water hypoxia has developed in the main channel in summer since 1971 (Wetsteyn, 2011).

Three sites, located along a water-depth gradient (sites 1-3, with water depths of 34, 23 and 17m respectively) in the Den Osse basin in the main channel of Lake Grevelingen (51.747°N, 3.890°E; 51.749°N, 3.897°E; 51.747°N, 3.898°E), were sampled monthly in 2012 on board

140 R/V Luctor (Figure 1). Sediment accumulation rates at sites 1, 2 and 3 were previously
141 estimated at ~2, 0.8 and 0.4 cm yr^{-1}, respectively (Malkin et al., 2014; Sulu-Gambari et al.,
142 2016b; Sulu-Gambari et al., 2016a). Discrete water column samples were collected at 8 water
143 depths (1, 3, 6, 10, 15, 25 and 32 m) using a 12 L Niskin bottle and gas-tight Tygon tubing.
144 Oxygen concentrations were measured in the collected samples using an automated Winkler
145 titration procedure (Hagens et al., 2015).

146 Bottom-water oxygen concentrations between 1978 and 2011 were available for site 1
147 through a monthly monitoring programme operated by the Ministry of Infrastructure and the
148 Environment (RWS) (Wetsteyn, 2011). Oxygen concentrations were assigned to specific time
149 intervals each year and assumed to start and end in the middle of the interval between
150 consecutive sampling dates. Each time interval was classified as 'anoxic' (< 1 µM oxygen),
151 'hypoxic' (1-62.5 µM oxygen), 'oxic' (> 62.5 µM oxygen) or 'not determined', depending on
152 the oxygen concentration and whether or not sampling was conducted.

153 Short sediment cores (~40 cm) with ~ 20 cm of overlying water were collected at the three
154 sites with a gravity corer (UWITEC, Austria) using Plexiglas® core-liners (6 cm inner diameter;
155 60 cm length). In addition to monthly sampling, a long core capturing the upper 90 cm of the
156 sediment was obtained with the UWITEC corer (6 cm inner diameter; 120 cm liner length) at
157 site 1 in May 2012. With an average sediment accumulation rate of ~2 cm yr^{-1} and duration of
158 the lake phase of ~41 years, since the closure of the system, the estuarine-lacustrine transition
159 in this core is expected near a depth of 82 cm.

160

161 **2.2. Sediment slicing, bottom-water and pore-water analyses**

The long core and the upper 10 cm of the sediment in each short core was sliced at a resolution of 0.5 cm in a N_2-purged glove-bag. Pore-water samples were collected through centrifugation of the sediment from the short cores (15 minutes at 4500 g). Pore-water data for major solutes, Fe, Mn (assumed to be Fe^{2+} and Mn^{2+}, although some Mn^{3+} may also be present; (Madison et al., 2013)), Ca^{2+} and SO_4^{2-} and nutrients for sites 1-3 are presented and discussed by (Sulu-Gambari et al., 2016b; Sulu-Gambari et al., 2016a). Here, we focus mainly on the water column and pore water at site 1 and include new data on trace metals, including high-resolution depth profiles. For sites 2 and 3, only water column data and discrete solid phase data are shown. Bottom- and pore-water samples for site 1 for January, March, May, June, July, August, September and November 2012, were filtered (0.45 µm) and sub-sampled under N_2 for various analyses. Subsamples were acidified with concentrated suprapur HCl (37%, 10 µl per ml), stored at 4°C and analysed for dissolved Fe, Mn and Ca by Inductively Coupled Plasma Optical Emission Spectrometry (ICP-OES; Perkin Elmer Optima 3000; detection limit < 0.01 ppm) and for dissolved Mo, Ni and V by ICP Mass Spectrometry (ICP-MS; Thermo Scientific X-series; detection limit < 0.3 ppb). Subsamples for sulphide (0.5 ml) were fixed with a 2% zinc-acetate solution (2 ml) and stored at 4°C. Sulphide was measured spectrophotometrically (Cline, 1969). A separate pore water aliquot was analysed for sulphate using a Dionex Ion Chromatograph.

2.3. Sediment Analyses

Centrifuged sediment samples from the short cores were freeze-dried and ground in a N_2-purged glove-box for analyses (January 2012 for sites 1 and 3 and March, May, August and November 2012 for all three sites). Selected data (sediment C_{org}, Mn, S) for sites 1, 2 and 3 were presented previously by (Sulu-Gambari et al., 2016b; Sulu-Gambari et al., 2016a). Here, we use these data to provide context for our trace metal analyses. The samples from the long core taken at site 1 in May 2012 were treated in the same manner as the short cores. The porosity of the

sediment was calculated from the weight loss upon freeze-drying assuming a sediment density of 2.6 g cm^{-3}. Total organic carbon (C_{org}) was measured using an elemental analyser (Fison Instruments, model NA 1500 NCS), after removing carbonate from the sediment with 1 M HCl. Total S, Fe, Mn, Mo, Al, Ni and V were determined by ICP-OES and verified by ICP-MS for those samples with measurements close to detection limits, following acid destruction of ground samples (~0.125 g) in a closed Teflon bomb at 90 °C (12 hr) using a mixture of 2.5 ml HF (40%) and 2.5 ml of a 72% $HClO_4$/ 65% HNO_3 mixture (volumetric ratio 3:2), evaporation of the acids at 190 °C and dissolution of the resulting gel in (25 ml) 1M HNO_3 (respective detection limits for Mn, Mo, Fe, Al, Ni and V were 0.03, 0.3, 54.2, 0.08, 0.05 and 0.2 ppb (ICP MS) and 0.28 ppm for S (ICP OES)) in the 1M HNO_3 solution).

2.4. Laser Ablation ICP-MS

Sub-cores of sediment (1 cm diameter, ~7 cm length) were taken from the surface sediment at site 1 in March and August 2012 as described by (Jilbert and Slomp, 2013a). The sediment in each sub-core was dehydrated with argon-purged acetone and fixed in Spurr's epoxy resin, and subsequently sliced into sections (~3.5 cm) with a water-cooled rotating blade for high-resolution elemental analysis and polished (Jilbert et al., 2008). Polished sections were analysed using Laser Ablation Inductively Coupled Plasma Mass Spectrometry (LA-ICP-MS) line scanning.

Elemental line scan profiles were generated by focussing a pulsed argon-fluoride excimer laser beam (120 μm spot size, 193 nm wavelength, 10 Hz repetition rate, and 8 J cm^{-2} energy density) onto the moving sample surface and ablating material into a high mass resolution ICP-MS (Thermo Element 2) in a continuously flowing helium-argon carrier gas. During line scans the stage velocity was set to 0.0275 mm s^{-1} for high spatial resolution measurements

211 (Hennekam et al., 2015). Count rates of isotopes ^{27}Al, ^{55}Mn and ^{98}Mo were determined, among
212 other isotopes, at a measurement frequency of approximately 1 Hz.

213 Line scans of each polished section were connected to construct a single record. The resin
214 embedding procedure results in varying degrees of sediment compaction, such that the length
215 of each line scan is less than the original ~7 cm sub-core. To correct for compaction effects, the
216 data from each LA-ICP-MS line scan was linearly re-scaled to the initial length of the sub-core.
217 Subsequently, line scan data were fine-tuned by alignment to ICP-OES dada of discrete samples
218 from the corresponding interval. Raw LA-ICP-MS count data were converted to elemental
219 compositional ratios as described in (Jilbert and Slomp, 2013a), with further modifications as
220 described by (Roepert et al., 2016).

221

222 **2.5. Suspended matter**

223 Water samples for suspended matter filtration were collected by Niskin bottle at site 1 as
224 described in section 2.1. During most months, water was transferred from the Niskin bottle to
225 2.5 L high-density polyethylene jerry cans, from which ca. 2500 ml was subsequently filtered
226 through pre-weighed, pre-combusted Whatman GF/F filters (nominal pore size 0.7 μm). In July
227 and August, when bottom waters were experiencing severe hypoxia/ anoxia, water below 10 m
228 depth was collected in volume-calibrated plastic bottles of ~2 L and filtered in a closed system,
229 to limit oxygen contamination. Filters were rinsed with UHQ water to remove sea salts and
230 stored at -20 °C until analysis.

231 The filters were freeze-dried and weighed, and suspended particulate matter concentrations
232 (mg L^{-1}) were calculated from the weight after freeze-drying and the total filtered volume of
233 water. After acid digestion, as described in Section 2.3, Mn concentrations were measured in
234 the HNO_3 solutions by ICP-OES. The acid solutions from water depths of 25 and 32 m for

April, May, June, July and August were additionally analysed for Mn and Mo by ICP-MS. The ICP-OES and -MS analyses for Mn always agreed within 5%. The Mn measurements were corrected for filter blanks (always less than 5% of Mn in suspended matter) and Mn concentrations were converted to ppm (mg per kg of solids). Given the high Mo blanks of the GF/F filters (5-75% of the Mo in the suspended matter), the Mo analyses for the suspended matter are approximations only and, therefore, we present only the average value for all 5 months.

2.6. Diffusive flux calculations

Diffusive fluxes of Mo at the sediment-water interface (J) were calculated from pore water profiles for site 1 using Fick's first law (Boudreau, 1997):

$$J = - \varphi D_s \frac{dC}{dx} \quad (1)$$

where φ is the porosity, D_s is the diffusion coefficient in the sediment, and $\frac{dC}{dx}$ is the gradient in the dissolved Mo concentration between the bottom water and the first sediment depth interval (where the distance to the midpoint is 0.25 cm). Diffusion coefficients in the sediment were calculated using the R *marelac* package (Soetaert et al., 2010), in which the 'difcoeff' function was modified to include Mo using the diffusion coefficient in seawater from (Li and Gregory, 1974). The 'difcoeff' function includes corrections for salinity, temperature and the tortuosity of the sediment (Boudreau, 1997). Downward fluxes of Mo into the dissolved sulphide-bearing zone were calculated in the same manner with the depth interval being determined by the depth at which dissolved sulphide was detected.

3. Results

3.1. Water column

Bottom-water oxygen concentrations displayed a clear seasonal cycle at all three sites in 2012 (Figure 2A). While oxygen concentrations were high (O_2 > 200 μM) in winter and autumn, they decreased in spring and summer (from May to August) at all three sites. Distinct differences were observed between sites 1 and 2 where the bottom water became hypoxic (O_2 < 62.5 μM) in summer, compared to site 3 where oxygen concentrations always remained above the threshold for hypoxia. Anoxia (O_2 < 1 μM) and the presence of sulphide in the bottom water (~3 μM) was only observed at site 1 in August.

Long-term monitoring data show that bottom-water anoxia was a regular feature in the basin in summer between 1979 and 1997 (Figure 2B). In contrast, between ~1998 and 2010, the bottom water was mostly hypoxic in summer. During the latter 12 year period, there was no clear trend in the duration of hypoxia. While a relatively long period of anoxia occurred in 2011 (Figure 2B), the duration of hypoxia was again comparably short in 2012 (Figure 2A).

Suspended matter concentrations at site 1 were highest in January and in late summer and autumn (Figure S1). Depth-integrated amounts of suspended matter in the water column ranged from ~65 to 230 g m^{-2} (Table S1). Concentrations of Mn in the suspended matter showed a strong seasonal variation, with highest concentrations near the lake bottom (> 40,000 ppm) in July and August (Figure 3). Weight ratios of Mo/Mn in the suspended matter, from water depths of 25 and 32 m (between April and August), average 0.0030 ± 0.0026.

3.2. Pore-water chemistry

High concentrations of Fe^{2+} and Mn^{2+} were observed in the upper 4 cm of the sediment at site 1 in January and March 2012 (Figure 4). Dissolved Fe^{2+} was low in June and then absent from the pore water from July onward, while Mn^{2+} concentrations were low during the rest of the

year. Sulphide was present in the pore water below 4 to 5 cm depth from January to May, but closer to the sediment surface in June and July (2 and 0.5 cm depth, respectively). In August, in contrast, sulphide was present in the bottom water (~3 μM). In November, a sulphide-free zone developed again but now in the upper 2 cm of the sediment. The shapes of the pore water profiles of Ca^{2+} and SO_4^{2-} are indicative of production of both solutes in the upper 4-6 cm of the sediment in January and March. For Ca^{2+}, profiles were nearly constant with depth from May onward. A decrease in pore water SO_4^{2-} with depth was observed in May, August and November.

Strong seasonal changes were observed in pore water Mo. In January and March, two subsurface maxima in pore water Mo were observed in the upper 4 to 6 cm of the sediment, with concentrations reaching ~300 nM. In May, June and July only one sharp maximum in Mo near the sediment-water interface was found, with concentrations reaching up to ~500 nM. In August, pore water Mo concentrations were very low and there was only a small enrichment near the sediment-water interface. In November, a slightly more distinct subsurface maximum in pore-water Mo (~130 nM) was present. Calculated diffusive fluxes of Mo across the sediment-water interface suggest release of Mo from the sediment during a major part of the year (Table 1). While the flux is near zero in March, an influx of Mo of 0.13 and 0.04 mg m^{-2} d^{-1} (1.4 and 0.4 μmol m^{-2} d^{-1}) is calculated for July and August, respectively. Downward diffusive fluxes of Mo into the sulphide-bearing zone ranged from 0.04 to 0.15 mg m^{-2} d^{-1}(0.4 to 1.6 μmol m^{-2} d^{-1}).

Both Ni and V were present in the pore water throughout the upper 10 cm of the sediment. Pore-water Ni was elevated in the upper ~4 cm of the sediment in January and March, but there were no other distinct trends with depth.

3.3. Bulk sediment chemistry

307 The sediments at all sites were rich in C_{org}, with concentrations ranging from 0.5 to 7 wt%
308 (Figures 5-7). At sites 1 and 2, concentrations of C_{org} oscillated with depth in the sediment, with
309 site 1 having fewer maxima than site 2. Such variations with depth were not observed at site 3.
310 While concentrations of Fe remained relatively constant with depth, there was a strong
311 seasonality in the concentrations of S and Mn in the surface sediment at all three sites. In spring,
312 the surface sediments at all sites were depleted in S and enriched in Mn relative to sediments at
313 depth. In August and November, the surface sediments at all sites were enriched in S while Mn
314 concentrations showed no change with depth. At site 1, distinct oscillations in concentrations
315 of S with depth were observed.

316 Concentrations of Mo in the surface sediment at sites 1 and 2 showed a distinct seasonality,
317 with low concentrations in January, March and May, high concentrations in August (up to 99
318 and 37 ppm, respectively) and either lower (site 1) or equally high concentrations (site 2) in
319 November. The depth profiles at both sites showed distinct enrichments in Mo that coincide
320 with maxima in the depth profiles of C_{org} and S. At site 3, Mo concentrations were very low (<
321 15 ppm) and showed little change with depth. There was a high background of Ni/Al and V/Al
322 in the sediment that was of a similar magnitude at all sites. Superimposed on this background,
323 distinct oscillations with depth were observed at sites 1 and 2 with maxima that coincide with
324 those of C_{org}, S and Mo.

325

326 **3.4. High-resolution solid-phase analyses**

327 LA-ICP-MS line scan profiles of Mn/Al and Mo/Al for March and August at site 1 confirm the
328 major seasonal changes in Mn and Mo in the surface sediment and the oscillations with depth
329 observed in the discrete sample data (Figure 8). Ratios of Mo/Mn (counts/counts) in the upper

mm of the sediment determined with LA-ICP-MS were 0.002 and 0.015, in March and August, respectively.

3.5. Long-term record of hypoxia

A distinct change in sediment geochemistry was observed at ~80 cm in the long core taken at site 1 in March 2012. This depth coincides with the depth of the expected estuarine-lacustrine transition based on the rate of sediment accumulation and suggests that at least the past 40 years of deposition in the lake are captured in this core. A distinct enrichment in C_{org} was observed in the surface layer of the long core taken in May 2012 at site 1 (Figure 9). The C_{org} content subsequently declined with depth to an oscillating background concentration of between 4 and 6 wt%. Distinct oscillations with depth were also observed in the profiles of total Fe, S and Mo but not in the profile of Mn. Background and peak Mo concentrations decreased with increasing depth, with the most pronounced maxima being observed in the upper 40 cm of the sediment.

4. Discussion

4.1. Impact of seasonal hypoxia on Mn dynamics

Low oxygen conditions in bottom waters in summer are a recurring phenomenon in Lake Grevelingen since the formation of the lake in 1971 (Figure 2; (Wetsteyn, 2011)). The hypoxia and anoxia are directly related to the combination of a stratified water column in summer and a high oxygen demand in the deeper waters and sediment. This oxygen consumption is fuelled by local production, re-deposition of organic-rich sediment from shallower areas and the input of organic matter from the North Sea through sluices in the seaward dam of the lake (Hagens et al., 2015; Seitaj et al., 2016).

353 The seasonal variations in bottom water redox conditions have major implications for
354 the biogeochemistry of the lake sediments (Seitaj et al., 2015; Sulu-Gambari et al., 2016b; Sulu-
355 Gambari et al., 2016a). Summer hypoxia has previously been shown to lead to the dissolution
356 of Mn oxides in the surface sediments at all three sites (Figures 5-7; (Sulu-Gambari et al.,
357 2016b)) and a loss of Mn from the sediment to the water column. While calculated diffusive
358 fluxes suggest a loss of Mn^{2+} from the sediment to the overlying water throughout the year
359 (with average Mn fluxes of ~ 80 mg m^{-2} d^{-1}at site 1(~ 1.45 mmol m^{-2} d^{-1} (Sulu-Gambari et al.,
360 2016b)), our suspended matter Mn data demonstrate that this release only leads to a strong
361 seasonal enrichment of Mn in suspended matter in the lake in summer (Figure 3). The integrated
362 amount of Mn in the water column in August at site 1 (~ 1200 mg m^{-2}; Figure 3, Table S1) is
363 more than a factor two lower than the amount released from the sediment, based on the seasonal
364 change in the surface enrichment in Mn (~ 2800 mg m^{-2}; assuming a sediment density of
365 2.6×10^6 g m^{-3} and measured porosity of 0.93; Figure 5). This suggests that some of the Mn in
366 the water column may be transported laterally out of the basin and/or may be re-deposited at
367 shallower water depths.

368 Due to the presence of oxygen in most of the water column (Figure 2 (Hagens et al., 2015)), the
369 particulate Mn in the suspended matter is assumed to be present as Mn oxides, formed by
370 oxidation of Mn^{2+} diffusing from the sediments into the water column. Refluxing of Mn likely
371 occurs throughout the summer, with gravity-driven settling of Mn-oxides fuelling further
372 reductive dissolution in the surface sediments as described for Chesapeake Bay (Adelson et al.,
373 2001a). We note one major difference with the Mn-refluxing observed in the latter system,
374 however, which relates to the location of Mn^{2+} oxidation. In Chesapeake Bay, the Mn^{2+} is
375 oxidised to Mn oxides just above the pycnocline in the water column and re-dissolved Mn^{2+} has
376 to diffuse back through the pycnocline to complete the reflux cycle (Adelson et al., 2001a). In
377 Lake Grevelingen, the pycnocline is located at a water depth of ~ 10 m in July and August

(Hagens et al., 2015) and most Mn oxides are formed well below the pycnocline (Figure 3). Because of the shorter diffusion pathway of Mn^{2+} before it meets oxygen, Mn cycling in the water column in Lake Grevelingen is likely more rapid than in Chesapeake Bay. We also note that suspended matter concentrations of Mn in Lake Grevelingen remain relatively high in autumn when compared to spring (Figure 3), while surface concentrations of sediment Mn show the opposite pattern (Figures 5-7). This suggests that Mn refluxing continues in autumn, although to a lesser extent than in summer.

4.2. Impact of seasonal hypoxia on Mo dynamics

The strong seasonality in Mn dynamics has major consequences for the dynamics of Mo in the lake sediments, because of the close association of Mo with Mn-oxides. We will illustrate this using the data for site 1. In late winter and spring, when the bottom water is oxygenated, surface sediments are enriched in Mn-oxides (Figure 5). The associated Mo enrichment is minor but detectable in the LA-ICP-MS line scan data (Figure 8). Pore water data for the same time of year show that Mn oxides are being dissolved at around 1-2 cm depth, releasing both Mn^{2+} and Mo, most likely mostly in the form of MoO_4^{2-} (Figure 4). Some of this Mo may escape to the overlying water through diffusion, especially in January, for which we calculate a diffusive flux out of the sediment of ~ 0.2 mg m^{-2} d^{-1} (1.9 µmol m^{-2} d^{-1} (Table 1). Given that there are only a few ppm of Mo in the surface sediment in spring (Figure 5 and 8) and 2 ppm sediment Mo over a depth of 1 cm would amount to ca. 3.6 mg m^{-2} (or 37 µmol m^{-2}; assuming a sediment density of 2.6×10^6 g m^{-3} and using the measured porosity of 0.93), this implies that the diffusive flux of Mo either is sustained only for several weeks or that there is a continuous recycling of both Mn and Mo through the water column near the sediment-water interface.

Upon the initial decline in oxygen in the bottom water in early summer (May and June), Mn oxide concentrations decline in the surface sediment (Figure 5) and increase in the suspended matter (Figure 3). However, a small sub-surface peak in pore water Mn (June) indicates that the ongoing input of Mn oxides to the sediments is followed by rapid dissolution (Figure 4). At this time, the release of Mo into the pore waters, and hence the efflux across the sediment-water interface, is at its highest value at any time of the year (0.6 and 1.4 mg m^{-2} d^{-1} or 6.2 and 1.5 µmol m^{-2} d^{-1} for May and June, respectively). Release of Mo from Fe-oxides may provide an additional source of Mo at this time of year (e.g. (Algeo and Lyons, 2006; Goldberg et al., 2012)). Coincident subsurface peaks of Fe^{2+} and Mn^{2+} in June support this suggestion (Figure 4).

When bottom waters are hypoxic and anoxic in July and August (Figure 1), pore water concentrations of Mo are low (Figure 4) and diffusive fluxes of Mo are directed into the sediments (Table 1). The sulphide concentration in the upper 0.5 cm of the sediment is ~725 µM. At a pH of ~7.4 (Sulu-Gambari et al., 2016b), this corresponds to a H_2S concentration of ~100 µM (Millero et al., 1988), which is greater than the concentration of 11 µM required for quantitative conversion of molybdate to tetrathiomolybdate and sequestration of Mo into the solid phase (Adelson et al., 2001b; Helz et al., 1996). The sediment Mo profile for August indeed shows a distinct enrichment of Mo in the upper cm of the sediment that reaches a maximum value of ~ 100 ppm. If the diffusive influx of July is assumed to be representative of the maximum influx for these two months and we assume an influx with a duration of 60 days, a total enrichment of Mo of only ~ 15 ppm in the upper cm can be achieved (assuming a sediment density of 2.6×10^6 g m^{-3} and the measured porosity of 0.98). This indicates that the diffusive influx of MoO_4^{2-} can only explain at most ca. 15% of the enrichment of Mo in the surface sediment at our site 1 in summer. We suggest that the remaining 85% of the Mo is supplied through input of Mn oxides from the overlying water.

426 Suspended matter near the bottom of the lake is highly enriched in Mn during July and
427 August (Figure 3). If we assume that this material has the same composition as the material
428 arriving at the sediment-water interface, it is possible to estimate whether Mn oxide input could
429 explain the observed surface-sediment enrichment in Mo at this time. With LA-ICP-MS, we
430 determined an Mo/Mn count ratio in oxic surface sediments of 0.002, which is similar to the
431 weight ratio calculated for sediments from a range of other sites (Shimmield and Price, 1986).
432 Our average Mo/Mn weight ratio in suspended matter was slightly higher at 0.003. Assuming
433 a Mn concentration in suspended matter of ~40,000 ppm and a Mo/Mn weight ratio of either
434 0.002 or 0.003), we calculate a Mo concentration of 80 or 120 ppm in suspended matter. This
435 suggests that indeed sufficient Mo can reach the sediment through Mn oxide deposition to
436 account for most of the Mo enrichment. Critical to this interpretation is that Mo is sequestered
437 after dissolution from Mn oxides, despite the loss of Mn itself from the sediments (Scholz et
438 al., 2013).

439 Upon re-oxygenation of the water column in autumn, the surface layer of the sediments
440 again contains some oxygen (Seitaj et al., 2016; Sulu-Gambari et al., 2016b). In November at
441 site 1, a smaller Mo peak is present near the surface than in August (Figure 5). While this could
442 be due to spatial variability in Mo accumulation, the smaller Mo peak could also indicate loss
443 of Mo due to post-depositional oxidation (Crusius et al., 1996), which may mobilise organic
444 and/or sulphide associated Mo. Hence, it is possible that the peaks in Mo deeper in the
445 sediments (3-4 peaks observed in the top 10 cm at site 1, Figure 5) represent past intervals in
446 which Mo has accumulated, then partially remobilised, leaving a remnant peak of lower
447 concentration.

448

449 **4.3. Seasonal hypoxia and sedimentary Mo sequestration**

450 The series of maxima in sedimentary Mo observed with depth at site 1 likely reflect seasonal
451 cycles of Mo sequestration, given the sediment accumulation rate of 2 cm yr^{-1}. Note that in
452 some cases Mo peaks may not represent the actual maxima upon deposition because of post-
453 depositional oxidation. That maxima in Mo are related to seasonal hypoxia is supported by three
454 additional lines of evidence. First, we observe similar Mo peaks at site 2, with the number of
455 peaks in the upper 10 cm of the sediment being a factor two higher, which is in accordance with
456 a sediment accumulation rate that is roughly half of that at site 1 (0.8 cm yr^{-1} versus 2 cm yr^{-1},
457 Figure 6). Second, we observe that both Ni/Al and V/Al show similar profiles to Mo at sites 1
458 and 2 (Figures 5 and 6). Since these trace metals are also known to be redox-sensitive
459 (Tribovillard et al., 2006), this supports the theory that seasonal changes in redox conditions
460 drive variability in Mo/Al. Third, such seasonal maxima in Mo have been reported previously
461 for another deep site in the lake (Egger et al., 2016). At this other site, the sediment
462 accumulation rate is exceptionally high (13 cm yr^{-1}) thereby likely excluding post-depositional
463 oxidation, and the magnitude of the Mo maximum has been shown to be directly correlated to
464 the area of hypoxia in the lake (Egger et al., 2016).

465 The importance of the Mn-oxide mechanism in controlling Mo sequestration in the lake
466 sediments is further illustrated by the distinct gradient in Mo concentrations in the sediment at
467 the three sites (Figure 10; up to 130 ppm at site 1 compared to 45 and 15 ppm at sites 2 and 3,
468 respectively). These sites are located along a gradient of increasing water depth and decreasing
469 bottom-water oxygen (Figure 2), and, likely, increasing Mn oxide deposition (Figure 3). While
470 there is a slight gradient in bottom water sulphide (3 µM at site 1; none at sites 2 and 3) in
471 August 2012, consistent with the gradient in water depth, the sulphide concentrations in the
472 upper 0.5 cm of the sediment pore water show a different trend. High sulphide concentrations
473 are found in this sediment layer at all sites in August (725 µM (Figure 4), ~1900 and ~220 µM
474 (Sulu-Gambari et al., 2016b) for sites 1, 2 and 3, respectively). At the prevailing pH values of

475 the pore water at these sites (~7.4-7.5), corresponding concentrations of H_2S are always greater
476 than 11 μM (Helz et al., 1996; Millero et al., 1988). Hence, the potential for Mo sequestration
477 based on the H_2S concentration (Helz et al., 1996) is expected to be similar at all sites in August,
478 and it is likely that contrasting Mo accumulation largely reflects variable supply of Mo by Mn
479 oxides. Surface-sediment Mn concentrations generally increase with increasing water column
480 depth (in the order site 1 > site 2 > site 3) due to the gravitational focussing of Mn oxides into
481 the deeper part of the basin during Mn refluxing (Figures 5 - 7). Hence, the higher supply of
482 Mo via Mn oxides at the deepest site determines the high concentrations in the sediments in
483 August.

484 The Mo concentrations at our site 1 are rather exceptional when compared to other
485 seasonally hypoxic marine environments. In fact, in the classification of Scott and Lyons
486 (2012), our summer values of up to 100 to 130 ppm at site 1 would fall within the range for
487 sediments with permanently euxinic bottom waters (> 100 ppm). We suspect that the strong Mn
488 refluxing at our site explains this unusual seasonal enrichment in Mo (also see discussion in
489 (Algeo and Lyons, 2006)). Figure 11 summarises our current understanding of the seasonal
490 dynamics of Mo fixation in the sediment at site 1, demonstrating the need for both a high input
491 of Mn oxides and high pore-water sulphide concentrations to allow for formation of Mo
492 enrichments, and the corresponding temporal evolution in the sediment Mo profiles.

493

494 **4.4. Impact of sulphide-oxidising bacteria on Mo dynamics**

495 As discussed in detail by Sulu-Gambari *et al*. (2016a) and Seitaj *et al*. (2015), various lines of
496 evidence including near-surface enrichments in pore water Ca^{2+} and SO_4^{2-} (Figure 4),
497 microprofiles of oxygen, sulphide and pH profiles characteristic for cable bacteria and
498 microscopic identification, point towards the presence of active cable bacteria at all three sites

499 in the spring of 2012. The enrichments in pore water Ca^{2+} and SO_4^{2-} are directly related to the
500 proton production associated with the electrogenic metabolism of the cable bacteria and have
501 been shown to be produced through dissolution of calcium carbonate and FeS at our field site
502 (Sulu-Gambari et al., 2016a), supporting results of earlier laboratory experiments (Risgaard-
503 Petersen et al., 2012). At site 1, cable bacteria have also been shown to contribute to dissolution
504 of Mn carbonates in the sediment (Sulu-Gambari et al., 2016b). Because part of the Mn^{2+} is
505 oxidised in the surface sediment, this enhances the pool of Mn oxides in the lake system
506 available for Mn refluxing.

507 In sediment with active cable bacteria, Mo associated with FeS would be expected to be
508 released to the pore water concurrently with the dissolution of FeS. At site 1, we indeed find a
509 distinct second maximum of pore water Mo in January and March (Figure 4) that could be
510 explained by such a dissolution process. The depth of the pore water Mo maximum coincides
511 with the maximum in pore water Ca^{2+}, which is located at a greater depth than the maximum in
512 Fe^{2+}. This difference could be related to a faster removal of downward diffusing Fe^{2+} with pore
513 water sulphide when compared to sulphide-driven fixation of Mo in the sediment. The ultimate
514 fate of the Mo is thus sequestration, but at a greater depth than before. We can only speculate
515 about the fate of the upward diffusing pore water Mo. One possibility is that it is bound to Fe-
516 oxides that are known to be present below the Mn-oxide-bearing layer (Sulu-Gambari et al.,
517 2016b; Sulu-Gambari et al., 2016a) and that their reduction contributes to the enhanced release
518 of Mo to the pore water in May and June.

519 In summary, our data suggest that, through their active oxidation of the sediment in spring,
520 cable bacteria could contribute to mobilisation of Mo deposited during the most recent prior
521 period of hypoxia, with the Mo either escaping out of the sediment or being sequestered again
522 at greater depth. The presence of cable bacteria could thus amplify the seasonal changes in
523 sediment Mo. Whether these processes have a significant impact on sediment Mo records is

difficult to deduce from the current data set and will depend on various factors, such as the rate of sediment accumulation at a given site, the depth to which FeS is removed and the initial amount of Mo associated with FeS. The downward fluxes of Mo (Table 1) when sustained over one month or more are sufficient to lead to measurable changes in Mo (~10 ppm). Given that at our sites 1 and 2, distinct oscillations in sediment Mo are visible, these processes clearly do not lead to removal of the Mo enrichments. However, they could lead to changes in peak height or smearing of Mo profiles. We also note that, prior to the establishment of the cable bacteria, Beggiatoaceae were active at all 3 sites in autumn and contributed to oxidation of the surface sediment. Although this oxidation did not extend as deep as in the presence of the cable bacteria, and some of the changes seen from month to month may be related to spatial variability (as suggested by the data for site 2; Figure 6), the activity of Beggiatoaceae may have contributed to mobilisation of Mo in the near surface sediment as well.

4.5. History of hypoxia

Lake Grevelingen has a history of several decades of seasonal hypoxia (Figure 2) which is reflected in oscillating concentrations of Mo, S and Fe in the sediment record for the past 40 years (Figure 10). To alleviate the hypoxia, the inflow of North Sea water at the seaward sluice was increased in 1999 (Wetsteyn, 2011). The increased inflow of this more saline, more oxygenated and warmer water indeed improved the oxygenation of the bottom waters in our study basin, mostly by reducing the temperature stratification in summer (Wetsteyn, 2011). As a consequence, anoxia in bottom waters generally became less frequent (Figure 2; (Wetsteyn, 2011)). Strikingly, however, the sediment Mo records suggest progressively sulphidic conditions in the pore waters towards the present day (Figure 9). We can reconcile these contrasting findings if we take into account that the inflowing North Sea water also carried large amounts of algal material (dominantly *Phaeocystis globosa*) into the lake in spring (Hagens et

549 al., 2015; Seitaj et al., 2016; Wetsteyn, 2011). The degradation of this organic matter likely
550 enhanced rates of sulphate reduction in late spring and summer, thereby increasing sulphide
551 concentrations in the pore water and enhancing the rate of Mn refluxing. Combined, these
552 factors could explain the increasing trend in sequestration of Mo at site 1. This sequence of
553 events is supported by the observation that the three major maxima in sediment Mo in the upper
554 32 cm of the long core coincide with maxima in organic carbon, with the maxima at ca. 32 cm
555 depth likely reflecting the input of organic matter in 1999. In summary, our sediment Mo record
556 reflects an increased input of organic matter and thus an increased oxygen demand of the
557 sediment. This demand is outpaced by an increased oxygen supply linked to the reduced
558 temperature stratification; bottom water anoxia in the basin has become less frequent.

559

560 **5. Conclusions**

561 Oscillations in molybdenum (Mo) in sediments in a seasonally-hypoxic marine basin (Lake
562 Grevelingen) reflect seasonal variations in the presence of sulphide near the sediment-water
563 interface and input of Mo with Mn-oxides. These results confirm the validity of Mo as a redox
564 proxy. Manganese recycling in the surface sediments and water column ("Mn refluxing") is
565 shown to play a key role as a carrier of the Mo to the sediment and explains the exceptionally
566 high Mo concentrations at one of our study sites (up to 130 ppm). Through their activity, cable
567 bacteria may modulate Mo records in our lake sediments by oxidising the surface sediment and
568 mobilising both Mn and Mo, but further research is needed to quantify these effects and assess
569 whether this plays a role in other marine systems. Oxygen measurements reveal an
570 improvement in bottom water oxygen conditions, related to increased flushing of the lake with
571 North Sea water since the late 1990s. This contrasts with the sediment Mo record for the deepest
572 site, which suggests periods of increased pore water sulphide concentrations between 1999 and

2012. These conflicting results are attributed to the input of fresh algal material (*P globosa*) in late spring and summer with the North Sea water, which likely fuelled additional sulphate reduction and sulphide production in the pore water and enhanced Mn refluxing and hence the supply of Mo to the sediment. Since the increased oxygen demand is outpaced by the increased oxygen supply associated with the flushing, the bottom-water oxygen conditions at the site have improved.

Acknowledgements

We thank P van Rijswijk, S Hidalgo, S van der Linde, C Lenz, the crew of the R/V Luctor (P Coomans and M Kristalijn) and various other members of the NIOZ and UU teams for their support during the sampling campaigns. We are also grateful to J Sinke, A Tramper, T Zalm and D van de Meent for analytical support, O Stiekema and L Bik for assistance with sample preparation and H de Waard for assistance with (LA-)ICP-MS analyses. This research was financially supported by the Darwin Centre for Biogeosciences, the European Research Council, under the European Community's Seventh Framework Programme (ERC Starting Grants 278364 to CPS and 306933 to FJRM), the Netherlands Organisation for Scientific Research (NWO Vici 865.13.005 to CPS) and the National Ocean and Coastal Research Programme (grant 83910502).

References

Adelson, J.M., Helz, G.R., Miller, C.V., 2001a. Reconstructing the rise of recent coastal anoxia; molybdenum in Chesapeake Bay sediments. Geochimica Et Cosmochimica Acta, 65(2): 237-252.

Adelson, J.M., Helz, G.R., Miller, C.V., 2001b. Reconstructing the rise of recent coastal anoxia; molybdenum in Chesapeake Bay sediments1. Geochimica et Cosmochimica Acta, 65(2): 237-252.

Algeo, T.J., Lyons, T.W., 2006. Mo–total organic carbon covariation in modern anoxic marine environments: Implications for analysis of paleoredox and paleohydrographic conditions. Paleoceanography, 21(1): PA1016.

601 Algeo, T.J., Tribovillard, N., 2009. Environmental analysis of paleoceanographic systems based on
602 molybdenum–uranium covariation. Chemical Geology, 268(3–4): 211-225.
603 Boudreau, B.P., 1997. Diagenetic Models and their Implementation. Springer, 414p pp.
604 Carstensen, J. et al., 2014. Hypoxia in the Baltic Sea: Biogeochemical Cycles, Benthic Fauna, and
605 Management. AMBIO, 43(1): 26-36.
606 Chappaz, A. et al., 2014. Does pyrite act as an important host for molybdenum in modern and ancient
607 euxinic sediments? Geochimica et Cosmochimica Acta, 126: 112-122.
608 Cline, J.D., 1969. Spectrophotometric determination of hydrogen sulfide in natural waters. Limnology
609 and Oceanography, 14(3): 454-458.
610 Collier, R.W., 1985. Molybdenum in the Northeast Pacific Ocean1. Limnology and Oceanography, 30(6):
611 1351-1354.
612 Crusius, J., Calvert, S., Pedersen, T., Sage, D., 1996. Rhenium and molybdenum enrichments in
613 sediments as indicators of oxic, suboxic and sulfidic conditions of deposition. Earth and
614 Planetary Science Letters, 145(1): 65-78.
615 Dahl, T.W. et al., 2017. Evidence of molybdenum association with particulate organic matter under
616 sulfidic conditions. Geobiology, 15(2): 311-323.
617 Diaz, R.J., Rosenberg, R., 2008. Spreading Dead Zones and Consequences for Marine Ecosystems.
618 Science, 321(5891): 926-929.
619 Egger, M. et al., 2016. Rapid Sediment Accumulation Results in High Methane Effluxes from Coastal
620 Sediments. PLOS ONE, 11(8): e0161609.
621 Emerson, S.R., Huested, S.S., 1991. Ocean anoxia and the concentrations of molybdenum and
622 vanadium in seawater. Marine Chemistry, 34(3): 177-196.
623 Erickson, B.E., Helz, G.R., 2000. Molybdenum(VI) speciation in sulfidic waters:: Stability and lability of
624 thiomolybdates. Geochimica et Cosmochimica Acta, 64(7): 1149-1158.
625 Freund, C. et al., 2016. The effect of a thiol-containing organic molecule on molybdenum adsorption
626 onto pyrite. Geochimica et Cosmochimica Acta, 174: 222-235.
627 Goldberg, T. et al., 2012. Controls on Mo isotope fractionations in a Mn-rich anoxic marine sediment,
628 Gullmar Fjord, Sweden. Chemical Geology, 296–297: 73-82.
629 Gooday, A.J. et al., 2009. Historical records of coastal eutrophication-induced hypoxia. Biogeosciences,
630 6(8): 1707-1745.
631 Hagens, M. et al., 2015. Biogeochemical processes and buffering capacity concurrently affect
632 acidification in a seasonally hypoxic coastal marine basin. Biogeosciences, 12(5): 1561-1583.
633 Helz, G.R., Adelson, J.M., 2013. Trace element profiles in sediments as proxies of dead zone history;
634 rhenium compared to molybdenum. Environ Sci Technol, 47(3): 1257-64.
635 Helz, G.R. et al., 1996. Mechanism of molybdenum removal from the sea and its concentration in black
636 shales: EXAFS evidence. Geochimica et Cosmochimica acta, 60(19): 3631-3642.
637 Hennekam, R., Jilbert, T., Mason, P.R.D., de Lange, G.J., Reichart, G.-J., 2015. High-resolution line-scan
638 analysis of resin-embedded sediments using laser ablation-inductively coupled plasma-mass
639 spectrometry (LA-ICP-MS). Chemical Geology, 403: 42-51.
640 Jilbert, T., De Lange, G.J., Reichart, G.-J., 2008. Fluid displacive resin embedding of laminated
641 sediments: preserving trace metals for high-resolution paleoclimate investigations. Limnology
642 and Oceanography: Methods, 6: 16-22.
643 Jilbert, T., Slomp, C.P., 2013a. Iron and manganese shuttles control the formation of authigenic
644 phosphorus minerals in the euxinic basins of the Baltic Sea. Geochimica et Cosmochimica acta,
645 107(0): 155-169.
646 Jilbert, T., Slomp, C.P., 2013b. Rapid high-amplitude variability in Baltic Sea hypoxia during the
647 Holocene. Geology, 41(11): 1183-1186.
648 Levin, L.A. et al., 2009. Effects of natural and human-induced hypoxia on coastal benthos.
649 Biogeosciences, 6(10): 2063-2098.
650 Li, Y.-H., Gregory, S., 1974. Diffusion of ions in sea water and in deep-sea sediments. Geochimica et
651 Cosmochimica Acta, 38(5): 703-714.

652 Madison, A.S., Tebo, B.M., Mucci, A., Sundby, B., Luther, G.W., 2013. Abundant Porewater Mn(III) Is a
653 Major Component of the Sedimentary Redox System. Science, 341(6148): 875-878.
654 Malcolm, S.J., 1985. Early diagenesis of molybdenum in estuarine sediments. Marine Chemistry, 16(3):
655 213-225.
656 Malkin, S.Y. et al., 2014. Natural occurrence of microbial sulphur oxidation by long-range electron
657 transport in the seafloor. ISME J.
658 Miller, C.A., Peucker-Ehrenbrink, B., Walker, B.D., Marcantonio, F., 2011. Re-assessing the surface
659 cycling of molybdenum and rhenium. Geochimica et Cosmochimica Acta, 75(22): 7146-7179.
660 Millero, F.J., Plese, T., Fernandez, M., 1988. The dissociation of hydrogen sulfide in seawater1.
661 Limnology and Oceanography, 33(2): 269-274.
662 Morford, J.L. et al., 2007. Insights on geochemical cycling of U, Re and Mo from seasonal sampling in
663 Boston Harbor, Massachusetts, USA. Geochimica et Cosmochimica acta, 71(4): 895-917.
664 Mort, H., Slomp, C., Gustafsson, B.G., Andersen, T.J., 2010. Phosphorus recycling and burial in Baltic
665 Sea sediments with contrasting redox conditions. Geochimica & Cosmochimica acta, 74: 1350-
666 1362.
667 Nielsen, L.P., Risgaard-Petersen, N., Fossing, H., Christensen, P.B., Sayama, M., 2010. Electric currents
668 couple spatially separated biogeochemical processes in marine sediment. Nature, 463(7284):
669 1071-1074.
670 Olson, L. et al., 2017. Trace metal diagenesis in sulfidic sediments: Insights from Chesapeake Bay.
671 Chemical Geology, 452: 47-59.
672 Paulij, W.P., Bogaards, R.H., Denucé, J.M., 1990. Influence of salinity on embryonic development and
673 the distribution of Sepia officinalis in the Delta Area (South Western part of The Netherlands).
674 Marine Biology, 107(1): 17-23.
675 Pfeffer, C. et al., 2012. Filamentous bacteria transport electrons over centimetre distances. Nature,
676 491(7423): 218-221.
677 Rabalais, N.N. et al., 2014. Eutrophication-Driven Deoxygenation in the Coastal Ocean Oceanography,
678 27.
679 Rabalais, N.N. et al., 2010. Dynamics and distribution of natural and human-caused hypoxia.
680 Biogeosciences, 7(2): 585-619.
681 Rao, A.M.F., Malkin, S.Y., Hidalgo-Martinez, S., Meysman, F.J.R., 2016. The impact of electrogenic
682 sulfide oxidation on elemental cycling and solute fluxes in coastal sediment. Geochimica et
683 Cosmochimica Acta, 172: 265-286.
684 Risgaard-Petersen, N., Revil, A., Meister, P., Nielsen, L.P., 2012. Sulfur, iron-, and calcium cycling
685 associated with natural electric currents running through marine sediment. Geochimica et
686 Cosmochimica acta, 92(0): 1-13.
687 Roepert, A., Jilbert, T., Slomp, C.P., 2016. Calibration of LA-ICP-MS line scan data to obtain high-
688 resolution geochemical records of resin-embedded sediment cores. Geochemistry,
689 Geophysics, Geosystems. Technical Reports: Methods: (submitted).
690 Scheiderich, K., Helz, G.R., Walker, R.J., 2010. Century-long record of Mo isotopic composition in
691 sediments of a seasonally anoxic estuary (Chesapeake Bay). Earth and Planetary Science
692 Letters, 289(1–2): 189-197.
693 Scholz, F., McManus, J., Sommer, S., 2013. The manganese and iron shuttle in a modern euxinic basin
694 and implications for molybdenum cycling at euxinic ocean margins. Chemical Geology, 355(0):
695 56-68.
696 Scott, C., Lyons, T.W., 2012. Contrasting molybdenum cycling and isotopic properties in euxinic versus
697 non-euxinic sediments and sedimentary rocks: Refining the paleoproxies. Chemical Geology,
698 324–325: 19-27.
699 Seitaj, D. et al., 2015. Cable bacteria generate a firewall against euxinia in seasonally hypoxic basins.
700 Proceedings of the National Academy of Sciences, 112(43): 13278-13283.
701 Seitaj, D. et al., 2016. Sedimentary oxygen dynamics in a seasonally hypoxic basin. Limnology and
702 Oceanography.

Shimmield, G.B., Price, N.B., 1986. The behaviour of molybdenum and manganese during early sediment diagenesis — offshore Baja California, Mexico. Marine Chemistry, 19(3): 261-280.
Soetaert, K., Petzoldt, T., Meysman, F., 2010. Marelac: Tools for aquatic sciences. R package version.
Sulu-Gambari, F. et al., 2016b. Impact of Cable Bacteria on Sedimentary Iron and Manganese Dynamics in a Seasonally-Hypoxic Basin. Geochimica et Cosmochimica Acta.
Sulu-Gambari, F. et al., 2016a. Cable Bacteria Control Iron–Phosphorus Dynamics in Sediments of a Coastal Hypoxic Basin. Environmental Science & Technology, 50(3): 1227-1233.
Tribovillard, N., Algeo, T.J., Lyons, T., Riboulleau, A., 2006. Trace metals as paleoredox and paleoproductivity proxies: An update. Chemical Geology, 232(1-2): 12-32.
Turekian, K.K., Wedepohl, K.H., 1961. Distribution of the Elements in Some Major Units of the Earth's Crust. Geological Society of America Bulletin, 72(2): 175-192.
Wagner, M., Chappaz, A., Lyons, T.W., 2017. Molybdenum speciation and burial pathway in weakly sulfidic environments: Insights from XAFS. Geochimica et Cosmochimica Acta, 206: 18-29.
Wedepohl, K.H., 1991. Chemical composition and fractionation of the continental crust. Geologische Rundschau, 80(2): 207-223.
Wetsteyn, L.P.M.J., 2011. Grevenlingenmeer: meer kwetsbaar?, RWS Waterdienst, Lelystad.
Zheng, Y., Anderson, R.F., van Geen, A., Kuwabara, J., 2000. Authigenic molybdenum formation in marine sediments: a link to pore water sulfide in the Santa Barbara Basin. Geochimica et Cosmochimica Acta, 64(24): 4165-4178.

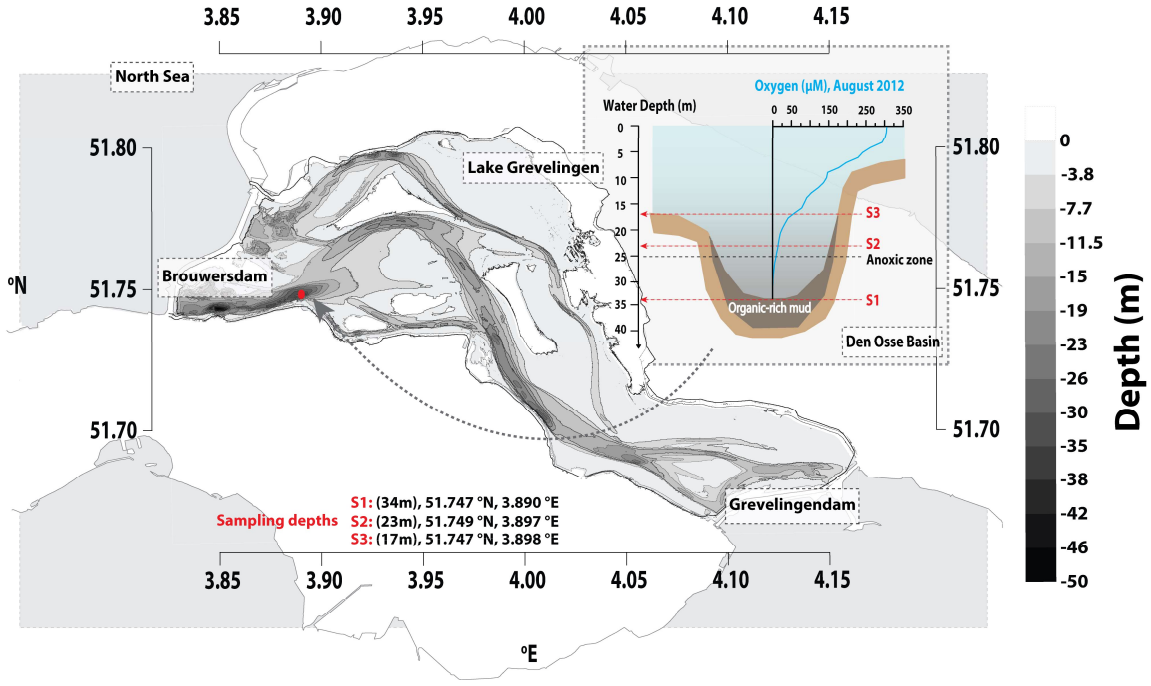

Figure 1: Location of the Den Osse basin at the south-western edge of Lake Grevelingen. Sediment samples were collected from three sites (S1-S3) along a water depth gradient from January to December 2012 (inset). The water column oxygen concentration as a function of water depth for site 1 is plotted for the most anoxic period of the sampling year, August 2012.

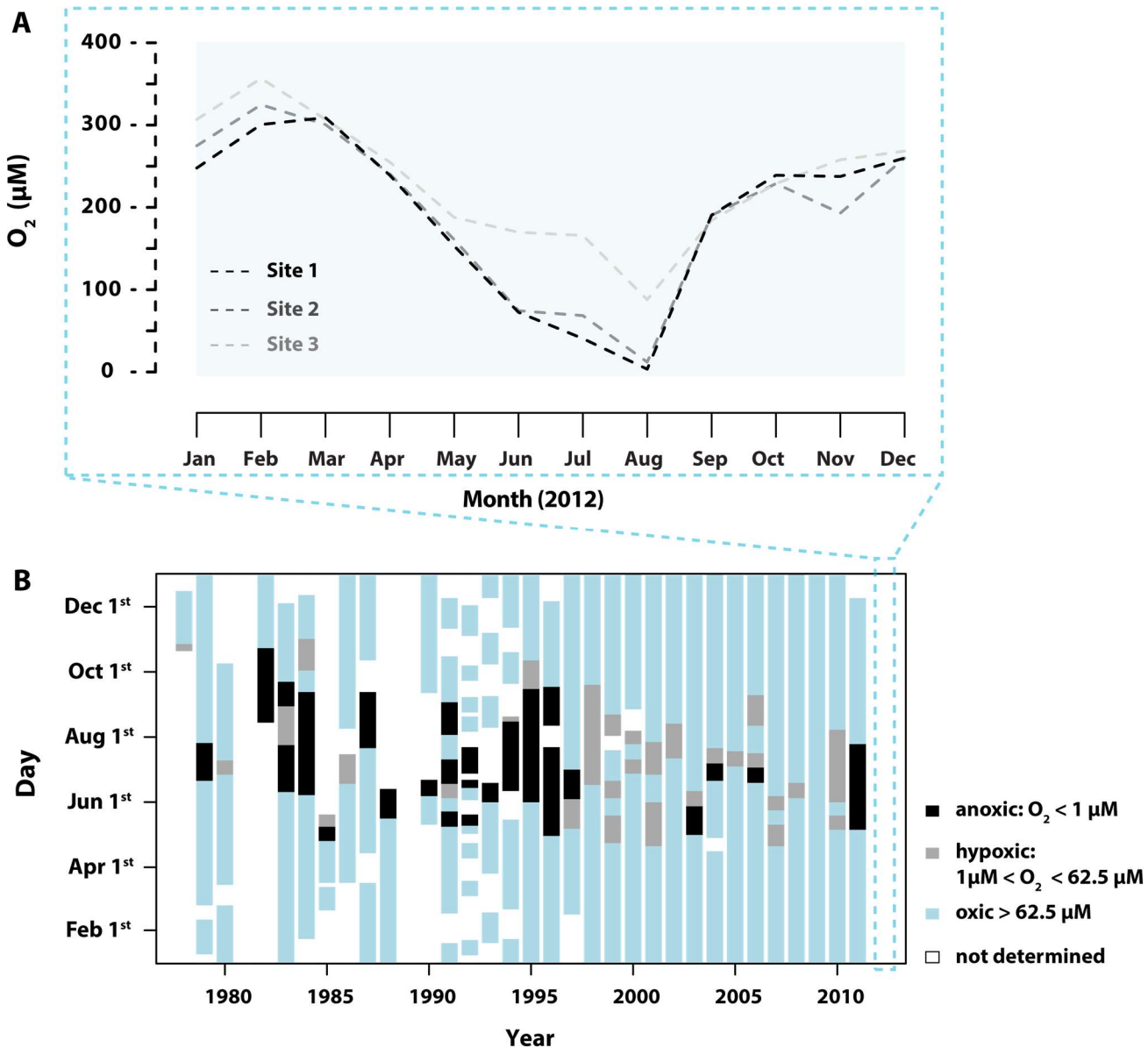

728

729 **Figure 2:** (A) Monthly bottom-water oxygen concentrations (in µM) at all three sites from January to December

730 2012. (B) Periods of oxic, hypoxic and anoxic bottom water conditions from 1999 to 2011 at site 1 (Ministry of

731 Infrastructure and Environment (Wetsteyn, 2011)).

732

733

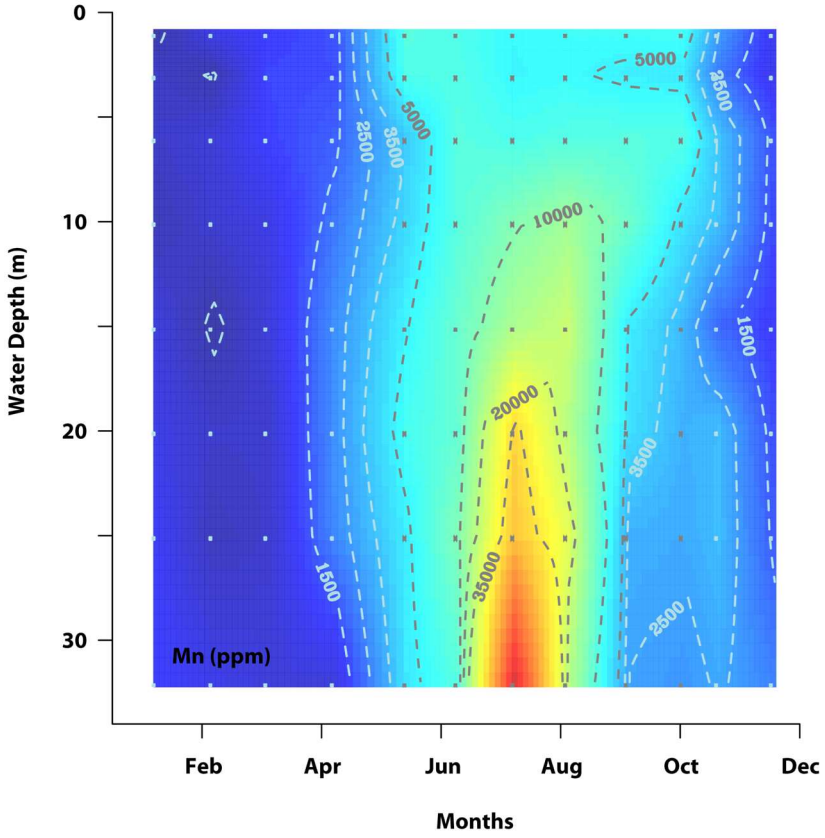

734

735 **Figure 3:** Concentrations of total Mn in suspended matter (in ppm) at site 1 for 2012. Note that a similar pattern
736 with depth and time is observed when Mn concentrations are expressed per volume of water; Figure S2). Data
737 are provided in Table S2.

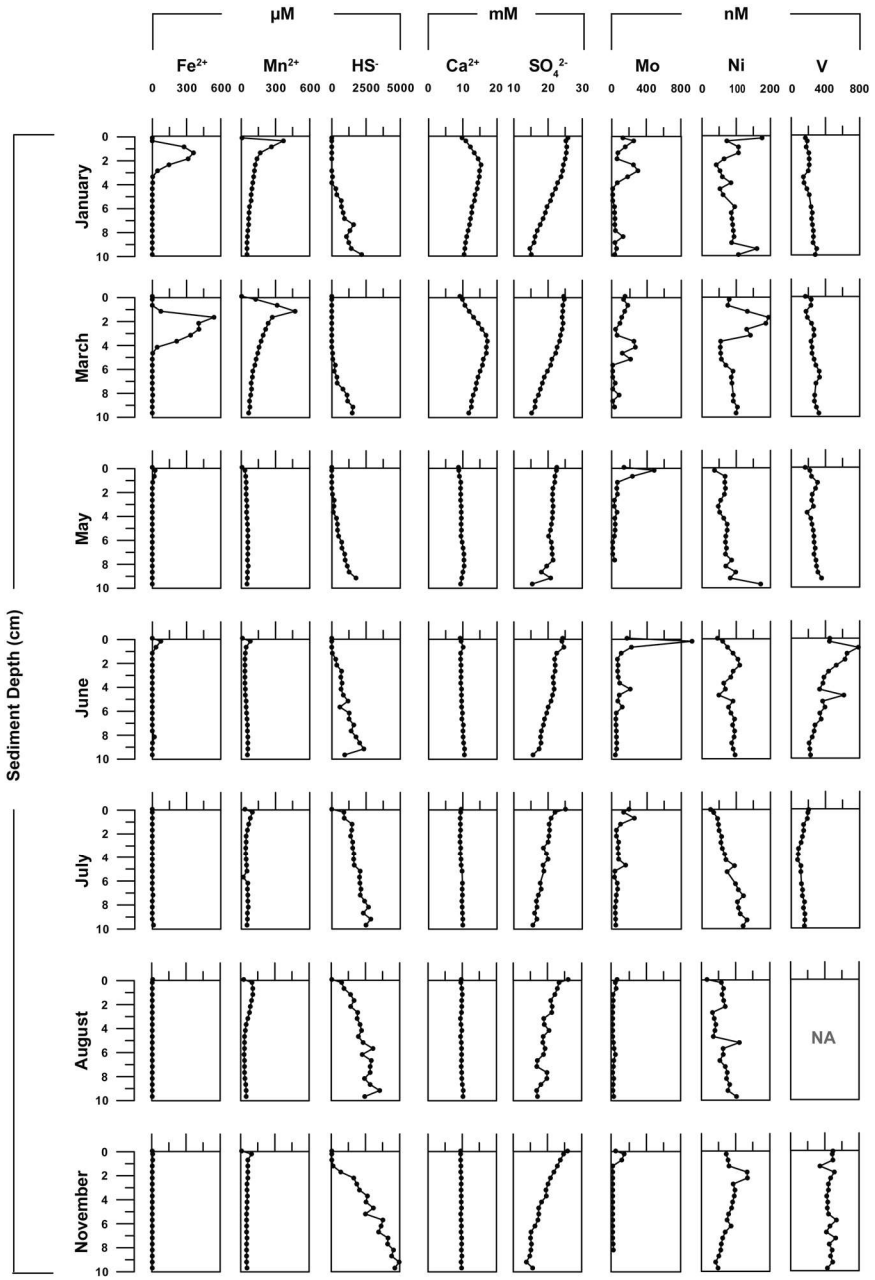

738

739 **Figure 4:** Pore water profiles of Fe^{2+}, Mn^{2+}, HS^-, Ca^{2+}, SO_4^{2-}, Mo, Ni and V for January, March, May, June, July,

740 August and November 2012 at site 1. Data are provided in Table S3.

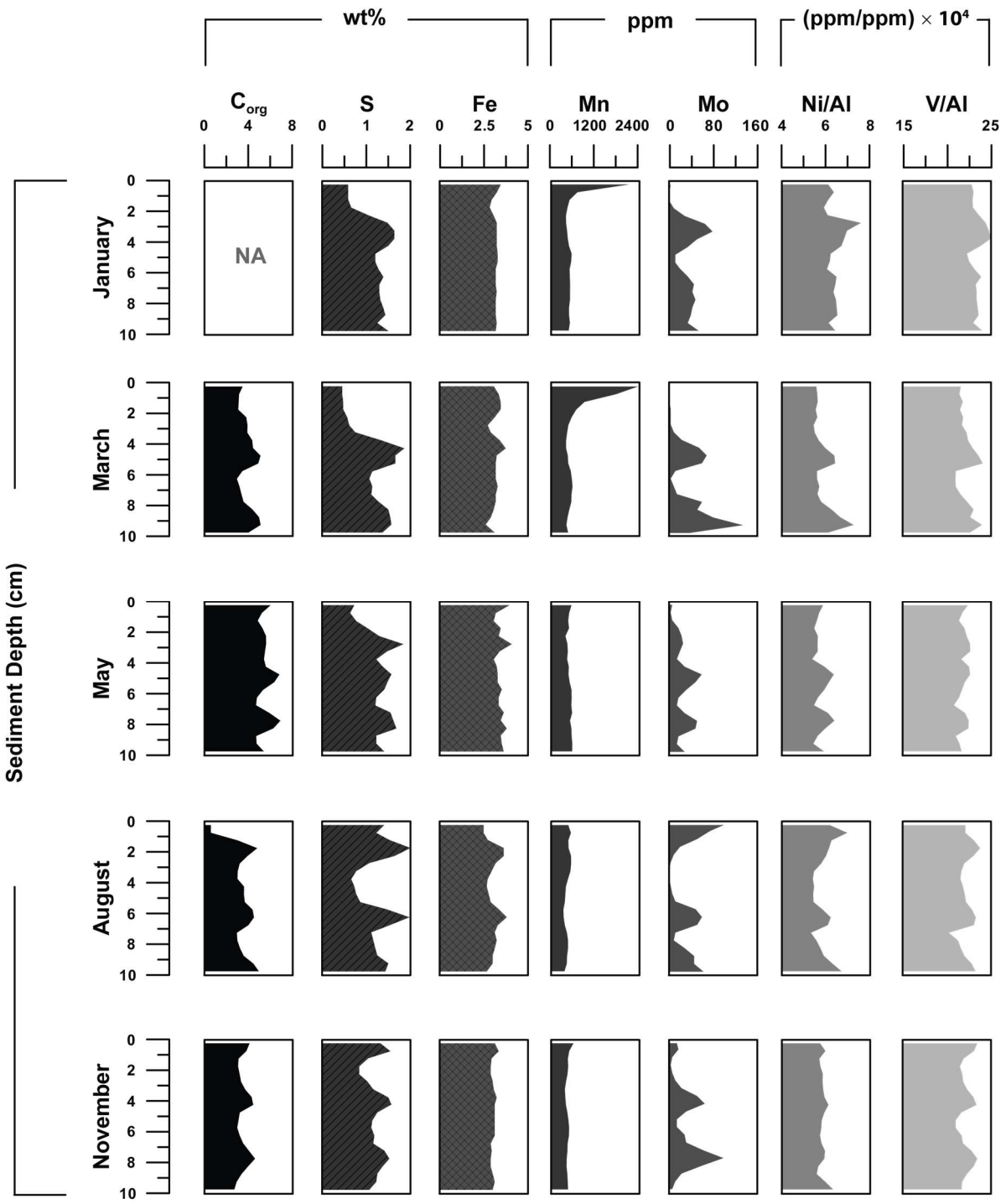

741

742 **Figure 5:** Sediment profiles of C_{org}, total S, Fe, Mn, Mo, Ni/Al and V/Al for January, March, May, August and
743 November 2012 at site 1. Nickel and vanadium are normalised to aluminium to account for the high background
744 concentration in clays (Wedepohl, 1991). Sediment profiles of Mo/Al are provided in Figure S3. Data are provided
745 in Table S4.

746

747

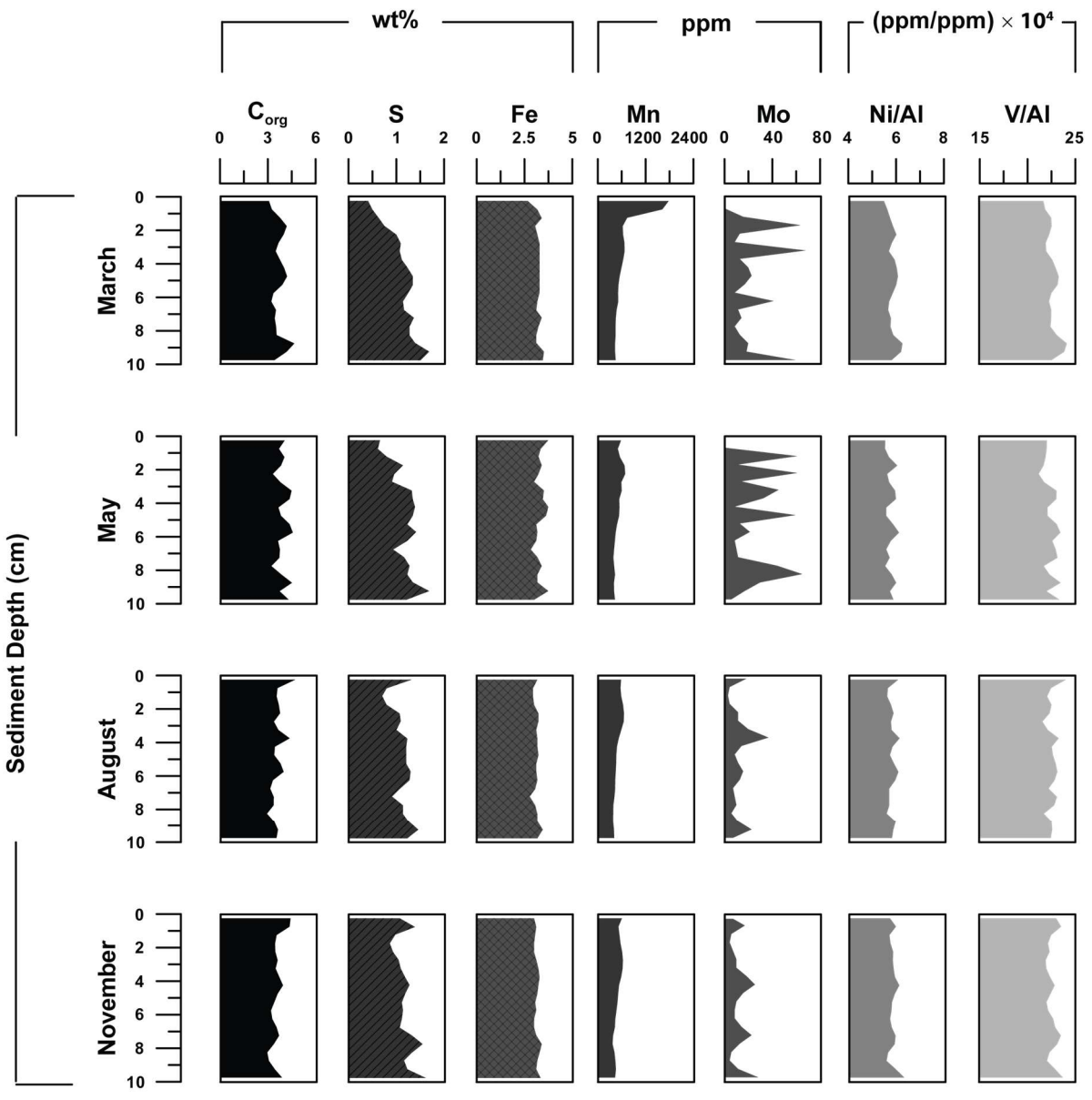

748

749 **Figure 6:** Sediment profiles of C_{org}, total S, Fe, Mn, Mo, Ni/Al and V/Al for March, May, August and November

750 2012 at site 2. Note that site 2 was not sampled in January 2012. Data are provided in Table S4.

751

752

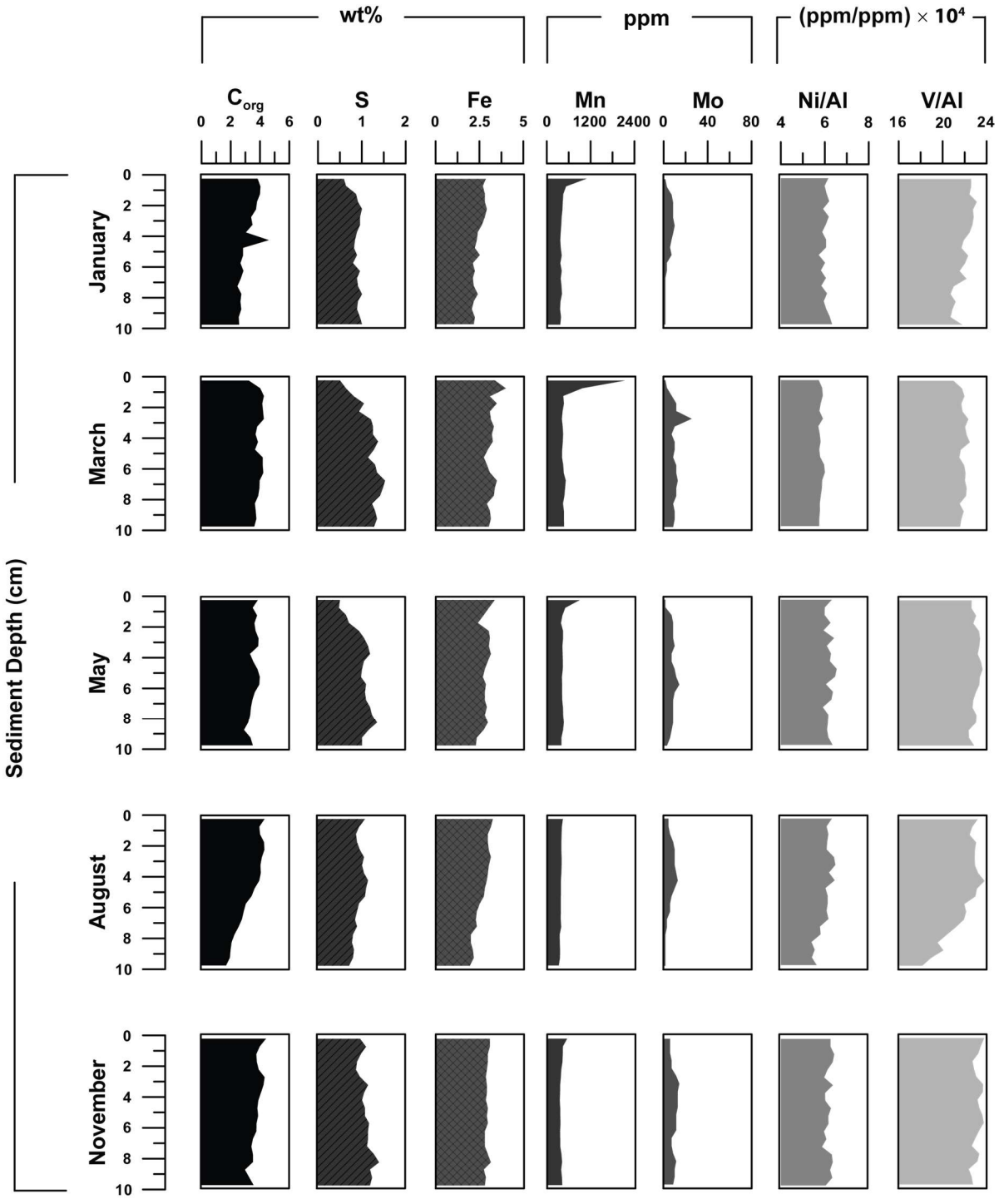

753

754 **Figure 7:** Sediment profiles of C_{org}, total S, Fe, Mn, Mo, Ni/Al and V/Al for March, May, August and November

755 2012 at site 3. Data are provided in Table S4.

756

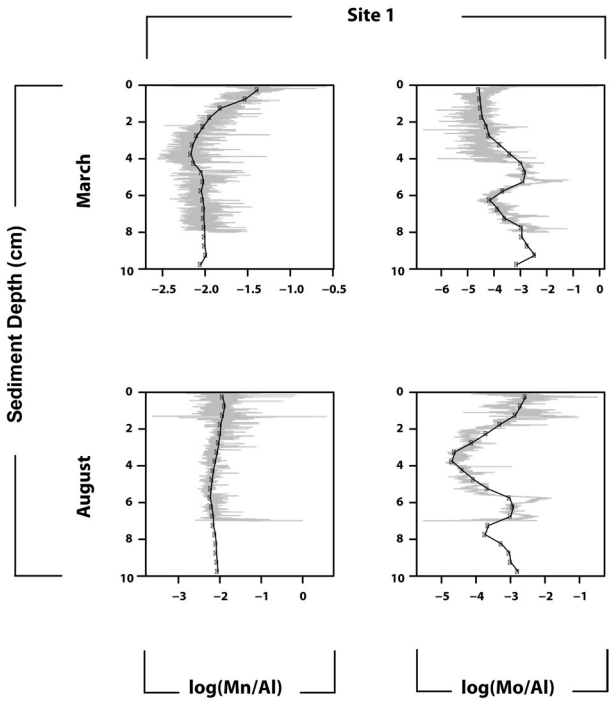

757

758 **Figure 8:** Sediment profiles of log(Mn/Al) and log(Mo/Al) for March and August 2012 at site 1 as obtained with
759 LA-ICP-MS (grey lines) and discrete sampling followed by total elemental analysis (black lines and dots). Data
760 are provided in Tables S6 and 7.

761

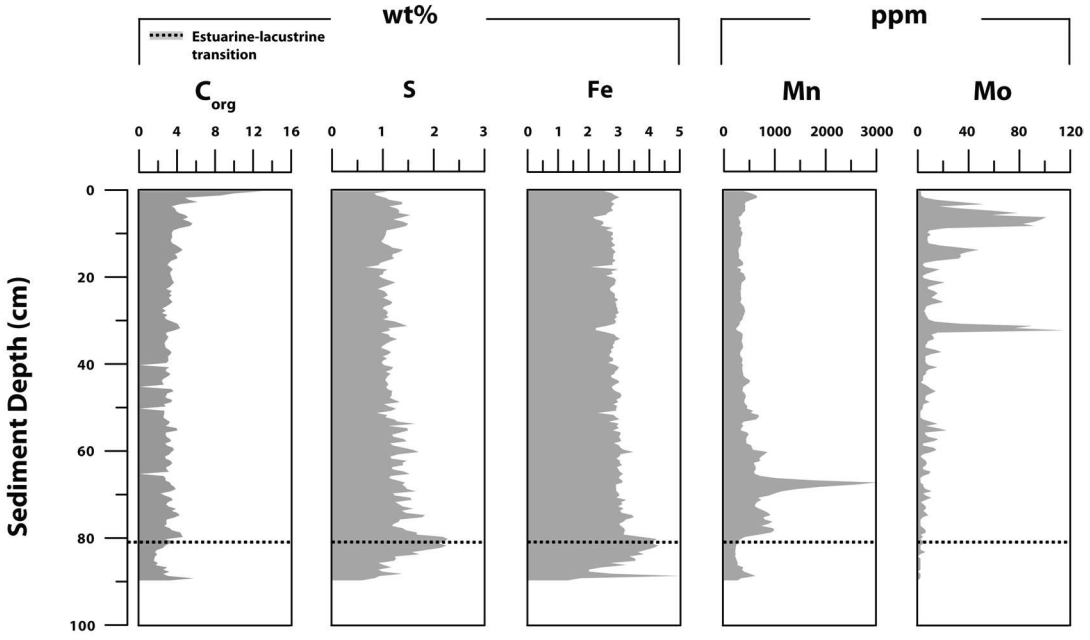

762

763 **Figure 9:** Sediment profile of C_{org}, total S, Fe, Mn andMo for the long core (90 cm) at site 1 for May 2012. The
764 estuarine-lacustrine transition is indicated with a dotted line. Data are provided in Table S5.

765 **Table 1:** Calculated diffusive molybdenum fluxes at the sediment-water interface (SWI) and deeper in the
766 sediment. *Calculated in R, with an adapted version of the marelac package (see section 2.6), using bottom water
767 salinity and temperature measurements from (Hagens et al., 2015). Positive fluxes are directed upwards, out of
768 the sediment.

Diffusive Fluxes Mo		SW I (0-0.25 cm)	Deeper flux	
Site 1	Diffusion Coefficient* (cm^2 s^{-1})	mg m^{-2} d^{-1}	Corresponding Depth Interval (cm)	mg m^{-2} d^{-1}
Jan	5.45E-06	0.19	3.75-4.25	-0.04
Mar	5.27E-06	-0.03	5.25-5.75	-0.15
May	6.07E-06	0.60	0.75-1.25	-0.14
Jun	6.21E-06	1.39	0.75-1.25	-0.11
Jul	7.12E-06	-0.13	1.25-1.75	-0.05
Aug	7.47E-06	-0.04	0.75-1.25	-0.04
Nov	6.62E-06	0.18	0.75-1.25	-0.10

769

770

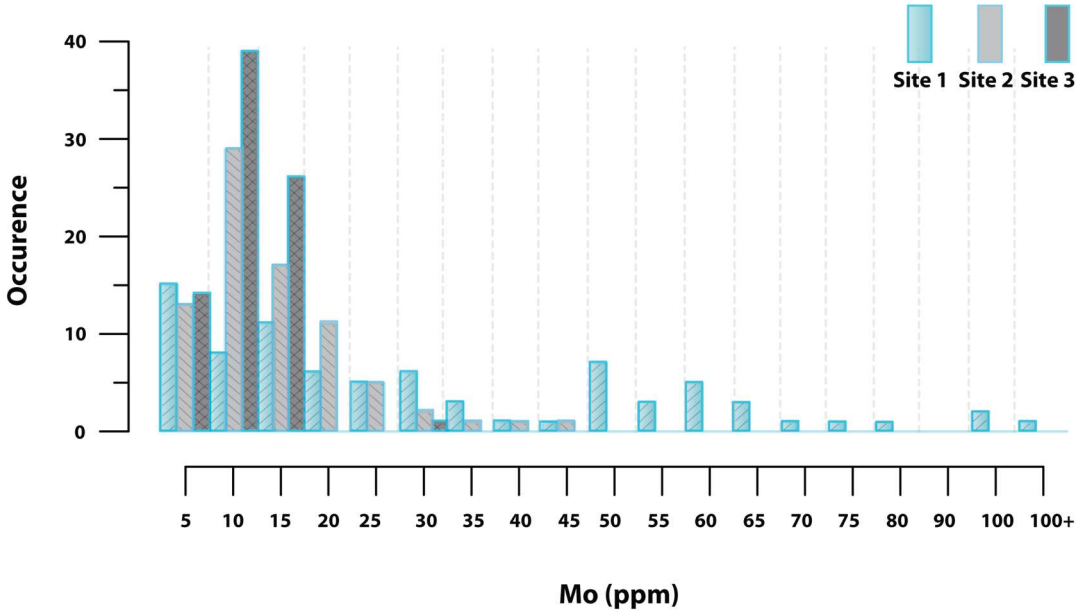

771

772 **Figure 10:** Number of samples with Mo concentrations (ppm) in different concentration ranges at sites 1-3 (after
773 (Scott and Lyons, 2012)). Where sulphide is present but restricted to the pore waters, sediment Mo concentrations
774 do not typically exceed 25 ppm. Conversely, in euxinic environments where hydrogen sulphide is present in the
775 water column throughout the year, and dissolved Mo is abundant due to effective exchange with the open ocean,
776 enrichments display a much wider range with concentrations consistently > 100 ppm (Scott and Lyons, 2012).

777

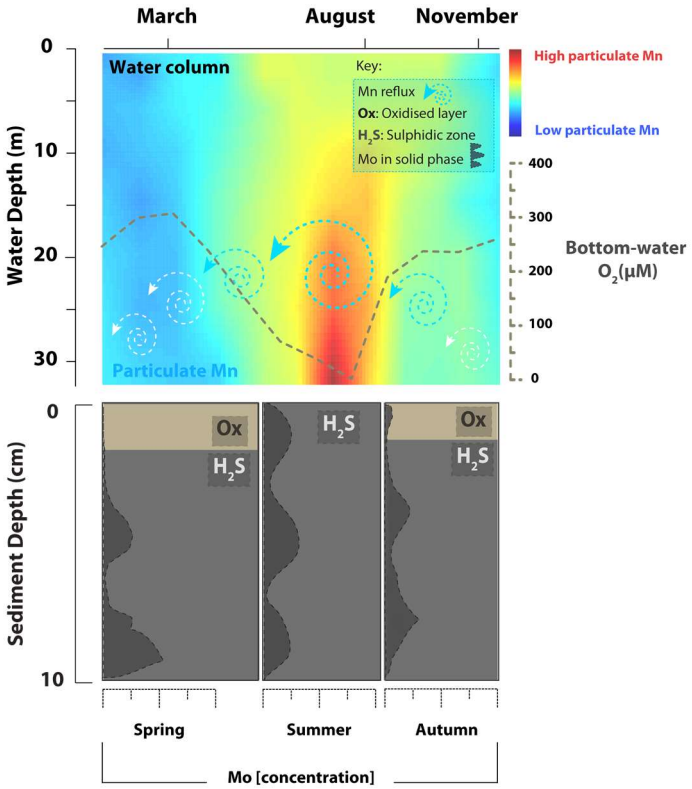

778

779 **Figure 11:** Schematic of Mo and Mn dynamics in the sediment and water column at site 1 in spring, summer and
780 late autumn. Upper panel: particulate Mn in the water column. Lower panel: schematic representation of sediment
781 Mo profiles.

782